

Reducing phenotype-structured partial differential equations models of cancer evolution to systems of ordinary differential equations: a generalised moment dynamics approach

Chiara Villa^{1,2} · Philip K. Maini³ · Alexander P. Browning³ · Adrianne L. Jenner⁴ · Sara Hamis^{5,6} · Tyler Cassidy⁷

Received: 3 September 2024 / Revised: 29 March 2025 / Accepted: 7 June 2025 / Published online: 28 July 2025 © The Author(s) 2025

Abstract

Intratumour phenotypic heterogeneity is understood to play a critical role in disease progression and treatment failure. Accordingly, there has been increasing interest in the development of mathematical models capable of capturing its role in cancer cell adaptation. This can be systematically achieved by means of models comprising phenotype-structured nonlocal partial differential equations, tracking the evolution of the phenotypic density distribution of the cell population, which may be compared to gene and protein expression distributions obtained experimentally. Nevertheless, given the high analytical and computational cost of solving these models, much is to be gained from reducing them to systems of ordinary differential equations for the moments of the distribution. We propose a generalised method of model-reduction, relying on the use of a moment generating function, Taylor series expansion and truncation closure, to reduce a nonlocal reaction-advection-diffusion equation, with general phenotypic drift and proliferation rate functions, to a system of moment equations up to arbitrary order. Our method extends previous results in the literature, which we address via three examples, by removing any a priori assumption on the shape of the distribution, and provides a flexible framework for mathematical modellers to account for the role of phenotypic heterogeneity in cancer adaptive dynamics, in a simpler mathematical framework.



22 Page 2 of 32 C. Villa et al.

1 Introduction

Intratumour heterogeneity is increasingly understood as a primary determinant of disease progression and therapeutic response in solid cancers (McGranahan and Swanton 2017; Burkhardt et al. 2022; Marine et al. 2020). While this heterogeneity has long-been viewed through the lens of clonal differences, recent experimental and clinical studies have implicated non-genetic heterogeneity as a driver of drug resistance and treatment failure (Bell and Gilan 2020; Hanahan 2022; Labrie et al. 2022). The Epithelial-Mesenchymal Transition (EMT) is a well-studied example of non-genetic resistance (Shi et al. 2023; Hanahan 2022), although a multitude of other examples exist, including adaptive rewiring of the mitogen activated protein kinase pathway (Labrie et al. 2022), and drug tolerant persisters in non-small cell lung cancer (Sharma et al. 2010; Goldman et al. 2015). Alongside its role in the development of drug-resistance, non-genetic plasticity is at the core of metabolic and morphological changes in cancer cells that facilite their metastatic spread and survival in harsh environments (Mosier et al. 2021; Shen and Clairambault 2020; Tasdogan et al. 2020).

Recent studies indicate that epigenetic regulation of genetically identical cancer cells induces a reversible drug-tolerant phenotype that expands during anticancer therapy (Kavran et al. 2022; Shaffer et al. 2017). In particular, transcriptomic data have identified reversible phenotypic changes that drive the development of resistance to targeted anti-cancer therapies and are mediated by a number of complex physiological factors (Kavran et al. 2022; Shaffer et al. 2017). Indeed, recent advances in multi-omics techniques have illustrated the complex dynamics of gene and protein expression that drive phenotypic plasticity (Chen et al. 2023; Tirosh et al. 2016). This ability to characterise population-level phenotypic plasticity permits a deeper understanding of evolution of non-genetic intratumour heterogeneity and the population distribution in phenotype space. Consequently, these experimental advances facilitate the development of mathematical models designed to capture both the shape and evolution of the phenotypic distribution of cancer cells.

Accordingly, there has been increased interest in the development of mathematical models to characterise the role of phenotypic heterogeneity in drug resistance and tumour progression (Clairambault and Pouchol 2019; Marusyk et al. 2020). A variety of deterministic and stochastic modelling frameworks have been proposed to study the evolutionary dynamics of phenotype-structured populations (Cassidy et al. 2021; Gunnarsson et al. 2020; Anderson et al. 2006; Stace et al. 2020). Many existing models of phenotypic plasticity have focused on characterising the dynamics of a fixed and finite number of phenotypes, with transitions between these discrete states corresponding to an evolutionary game (Kareva 2022; Craig et al. 2019; Kaznatcheev et al. 2019; West et al. 2018). This discrete-phenotype framework is particularly common in the study of cancer treatment and relies on the assumption of the existence of drug-sensitive and drug-resistant subpopulations (Smalley et al. 2019; Craig et al. 2019; Cassidy and Craig 2019). However, as the role of continuously increasing levels of drug resistance has become apparent in driving treatment response, there has been increased interest in understanding the adaptive dynamics that drive short-term phenotypic adaptation in response to, for example, the application of chemothera-



peutic drugs. Moreover, the relevance of capturing phenotypic variants on a continuum extends beyond the study of the development of drug resistance, as phenotypic changes in cells are mediated by variations in the level of expression of relevant genes and proteins, which are indeed measured on a continuum.

Dieckmann and Law (1996) proposed an adaptive dynamics framework to explicitly capture the dynamics of the continuous adaptation of the mean phenotypic state, with population level heterogeneity captured by means of stochastic fluctuations in phenotype space, specifically focusing on 'mutation-selection' dynamics which are easily transferable to the study of cancer (Aguadé-Gorgorió and Solé 2018; Martinez et al. 2021). Moreover, their derivation of an ODE system for the dynamics of the mean evolutionary path inspired many deterministic studies, generally more amenable to analytical investigations (Gunnarsson et al. 2020; Altrock et al. 2015), of adaptive dynamics relying on the simplifying assumption of a monomorphic population (Coggan and Page 2022; Martinez et al. 2021; Vincent and Brown 2005). These models often comprise a system of ordinary differential equations (ODEs) that model the evolution of both the population size and the mean trait $m_1(t)$. Nonetheless, as increasing importance is being attributed to population-level heterogeneity, we focus on deterministic frameworks providing a mean-field macroscopic description of stochastic, individual-cell dynamics, that do not rely on the limiting assumption of a monomorphic population.

The resulting modelling approach typically describes the time-evolution of the entire phenotypic density function, denoted p(t, x). The dynamics of the population, which is continuously structured by the variable x in phenotype space, are modelled by a nonlocal partial differential equation (PDE) which typically takes the form of a reaction-advection-diffusion equation. Equations of this type may be studied with the theory of semigroups of operators, fixed point theorems in Banach spaces, and numerical methods, with semi-classical asymptotic methods having become increasingly popular to study certain limit cases (Chisholm et al. 2016c; Dieckmann and Law 1996; Düll et al. 2021; Perthame 2006; Perthame and Barles 2008).

This framework explicitly captures the continuous phenotypic adaptation of the population while preserving information on population-level heterogeneity, and is becoming increasingly common as experimental advances allow for direct characterisation of cancer cell phenotypes. For example, Almeida et al. (2024) and Celora et al. (2022) leveraged time-resolved flow cytometry experiments to inform a structured PDE model of adaptation to nutrient or oxygen deprivation. Notably, in these works the phenotypic state x is interpreted as the level of expression of a certain gene or protein, although this need not be the case (Chisholm et al. 2015; Cho and Levy 2018b).

Although phenotype-structured PDEs carry increased biological relevance in the context of heterogeneous tumours, they pose a set of challenges that do not apply to standard ODE modelling frameworks. For example, it is possible to establish the existence of equilibrium solutions of these PDE models via fixed point approaches in an appropriate Banach space. However, this fixed-point approach may not be constructive and is more mathematically involved than calculating equilibrium solutions of ODE models, which typically only involves solving a possibly non-linear set of equations. In addition, numerical methods for PDEs are typically implemented on a case-



by-case basis, while highly efficient and accurate solvers for ODEs are found in most software packages. As parameter estimation typically involves many model simulations, the increased numerical efficiency of solving ODE is magnified when calibrating these models against experimental data. Multi-omics approaches that characterise the phenotypic distribution of tumours are becoming increasingly common. Nevertheless, experimental machines providing a full characterisation of gene and protein expression distributions (e.g. via flow cytometry or mass spectronomy) are yet to be widely available in experimental facilities due to their elevated cost, and more accessible techniques (e.g. Western blotting or RNA-seq) may only describe lower order moments- such as the mean and variance- of the phenotype distribution. Here, we develop a technique to reduce phenotype-structured PDEs to a system of ODEs for the moments characterising the phenotypic density function p(t, x). This reduction will allow modellers to use existing technical tools for ODE models, such as those for identifiability analysis, sensitivity analysis, and model parameterisation, while maintaining the biological relevance and interpretability of the phenotype-structured PDE. A similar approach has been applied in mathematical oncology (Almeida et al. 2024; Ardaševa et al. 2020; Lorenzi et al. 2015; Villa et al. 2021), generally building on the model reduction procedure developed by Almeida et al. (2019) and Chisholm et al. (2016b). There, the authors showed that if the initial phenotypic density distribution, with $x \in \mathbb{R}$, is normally distributed with mean $m_1(0)$ and variance $\sigma^2(0)$, then under further restrictions on the population net-proliferation rate and phenotypic drift rates, it is possible to obtain explicit ODEs for $m_1(t)$ and $\sigma^2(t)$. However, while protein expression distributions may be approximately normal in some cases (Almeida et al. 2024), the assumption that the phenotypic trait x is unbounded and possibly negative is not, in general, compatible with biological data. Moreover, the additional restrictions on the functional forms of terms relating to proliferation rate and phenotypic drift in these studies reduce the model applicability to a limited range of biological scenarios.

Here, we propose a generalised method to reduce phenotype-structured PDEs modelling cell adaptive dynamics to a system of ODEs for the moments characterising the phenotypic density function p(t, x). Our method allows us to extend the analysis presented in Almeida et al. (2019); Chisholm et al. (2016b); Lorenzi et al. (2015) by:

- (i) Relaxing the assumption of an unbounded phenotype space, thus working in a more biologically relevant phenotypic domain;
- (ii) Removing all a priori assumptions on the shape of the distribution;
- (iii) Removing the additional restrictions on the phenotypic drift and net proliferation rate terms.

The model reduction procedure relies on the use of the moment generating function of the phenotypic distribution and techniques such as Taylor series expansion and moment closure that have previously been used in the stochastic modelling literature (Engblom 2006; Kuehn 2016; Fan et al. 2016; Schnoerr et al. 2017; Wagner et al. 2022). We thus obtain a system of ODEs for the moments characterising the phenotypic density function up to an arbitrary order. The remainder of the manuscript



is structured as follows. After introducing the general phenotype-structured reactionadvection-diffusion equation in Sect. 2, we demonstrate the model reduction procedure in Sect. 3, compare results with several examples from the extant literature in Sect. 4, before concluding with a discussion in Sect. 5.

2 A general phenotype-structured PDE model of cell adaptive dynamics

Let p(t, x) denote the phenotypic density function of the population at time t, i.e. the density of cells in the phenotypic state $x \in \Omega \subset \mathbb{R}$ at time $t \in \mathbb{R}_{\geq 0}$, with $\Omega := [l, L] \ (0 < l < L)$ a compact and connected set. The population size at time t, P(t), is obtained by integrating over all possible phenotypes and is given by

$$P(t) = \int_{\Omega} p(t, x) dx. \tag{1}$$

We assume that p(t, x) satisfies the following PDE

$$\partial_t p(t,x) - \beta \partial_{xx}^2 p(t,x) + \partial_x \left[V(t,x) p(t,x) \right] = \left(f(t,x) - \frac{P(t)}{\kappa} \right) p(t,x), \quad (2)$$

for t>0 and $x\in\Omega$. Eq. (2) is complemented with no flux boundary conditions

$$\beta \partial_x p + V(t, x)p = 0 \quad \text{for} \quad x \in \partial \Omega,$$
 (3)

where we denote the boundary of Ω by $\partial\Omega$, and the initial condition

$$p(0,x) = p^0(x) \geqslant 0$$
, with $\int_{\Omega} p^0(x) dx > 0$, (4)

where $p^0(x)$ denotes the phenotypic density function at time zero.

The second term on the left-hand-side of Eq. (2) models spontaneous phenotypic changes as a diffusive flux (Chisholm et al. 2016b, a; Cho and Levy 2018a) with constant diffusion coefficient $\beta \ge 0$. The third term on the left-hand-side of Eq. (2) models environment-driven phenotypic changes by an advection term (Almeida et al. 2024; Celora et al. 2021) with velocity V(t, x), the time-dependency of which is likely mediated by some environmental factor denoted by $c(t) \ge 0$, i.e. $V(t,x) \equiv V(c(t),x)$. The reaction term on the right-hand-side of Eq. (2) models phenotype-dependent cell proliferation and death as in the non-local Lotka-Volterra equation (Perthame and Barles 2008). The phenotype-dependent intrinsic growth rate f(t, x) is likely mediated by some environmental factor c(t), i.e. $f(t,x) \equiv f(c(t),x)$, while the rate of death due to competition for space depends on the population size P(t), defined in (1), and the constant carrying capacity coefficient $\kappa > 0$.

We assume that the functions f(t, x) and V(t, x) are continuous in x at each point in time, i.e.



22 Page 6 of 32 C. Villa et al.

$$f(t,\cdot) \in C^0(\Omega)$$
 and $V(t,\cdot) \in C^0(\Omega)$, $\forall t \in \mathbb{R}_{\geq 0}$, (5)

and bounded in t for each phenotypic state, i.e.

$$f_m \leqslant f(\cdot, x) \leqslant f_M$$
 and $V_m \leqslant V(\cdot, x) \leqslant V_M$, $\forall x \in \Omega \subset \mathbb{R}$. (6)

Models comprising PDEs in the form of Eq. (2) can be formally derived from stochastic individual based models in the continuum, deterministic limit, see for instance (Champagnat et al. 2002, 2006; Chisholm et al. 2016b; Stace et al. 2020) and references therein. In particular, the diffusion and drift terms emerge as the macroscopic deterministic description of a biased random walk (Chisholm et al. 2016b; Lorenzi et al. 2020; Stace et al. 2020). In the stochastic and statistical literature, the left-hand-side of Eq. (2) is usually thought of as a Fokker-Planck equation (or equivalently, a Kolmogorov forward equation) (Kadanoff 2000), which arises as the governing equation for the probability density function of a set of non-interacting particles undergoing a biased diffusion process in x.

Remark 2.1 The phenotypic state x of a cell can be interpreted directly as the cellular level of expression of some gene and/or protein which mediates the observable characteristics and behaviour of the cell, relevant to the specific problem of interest. Due to natural biological constraints, gene and protein expression levels live in a bounded domain, as already clarified in the Introduction, motivating the choice of $\Omega := [l, L] \subset \mathbb{R}$. The value of l and L, i.e. the lowest and highest gene/protein expression levels realistically admissible, should be carefully selected by the modeller and inferred from biological data. In practice, these bounds encompass the entirety of the observable data. Consequently, gene/protein expression levels outside Ω are expected to be biologically infeasible and can be neglected.

3 Reduction to a system of ODEs characterising the phenotypic distribution

The structured PDE (2) captures the dynamics of the density of cells in phenotypespace. However, the density of cells with a given phenotype is unlikely to be the object of experimental or clinical interest. Rather, the evolution of the population size and distribution in phenotype space is relevant for understanding phenotypic adaptation. Consequently, we now generate a system of ODEs to characterise the population distribution in phenotype space. We begin by considering the size of the total population, P(t).

3.1 The total cell population

The population size P(t) only depends on time due to the integration over phenotype space. We can therefore derive an integro-differential equation for the population size P(t).



Lemma 3.1 Let p(t, x) satisfy Eq. (2), with f satisfying assumption (6), along with boundary conditions (3), initial conditions (4) and definition (1). The population size P(t) evolves according to the integro-differential equation

$$\frac{\mathrm{d}}{\mathrm{d}t}P(t) = \int_{\Omega} f(t,x)p(t,x)\mathrm{d}x - \frac{P^2(t)}{\kappa},\tag{7}$$

complemented with the initial condition

$$P(0) = \int_{\Omega} p^0(x) \mathrm{d}x > 0. \tag{8}$$

Moreover, under the assumption in Eq (5), we have that

$$0 < P(t) \leqslant \overline{P} < \infty, \quad \forall t \geqslant 0. \tag{9}$$

The proof follows standard calculations, cf. Appendix A.

3.2 The moment generating function

In Lemma 3.1, we derived an integro-differential equation for the population size P(t). However, this integro-differential equation explicitly depends on the phenotypic density function. Rather than studying this explicitly, we instead characterise p(t, x) by recasting it as a probability distribution in phenotype space and studying the moments of this distribution. Hence, in what follows, we consider the phenotypic density function scaled by the total population size

$$\hat{p}(t,x) = \frac{p(t,x)}{P(t)}. (10)$$

The distribution $\hat{p}(t, x)$ encodes a time-dependent probability measure $\mu(t)$ over phenotype space. This measure $\mu(t)$ has a Radon-Nikoydym derivative with respect to the Lebesgue measure λ given by the distribution $\hat{p}(t, x)$, i.e.

$$\frac{\mathrm{d}\mu}{\mathrm{d}\lambda} = \hat{p}(t, x).$$

This measure $\mu(t)$ and the population size P(t) is sufficient to describe the phenotypestructured population p(t, x). In what follows, we develop a system of ODEs to characterise the moments of the distribution $\hat{p}(t,x)$; Curto and di Dio (2023) performed a similar analysis for the heat equation. We consider the moment generating function of the distribution $\hat{p}(t, x)$, given by

$$M(s,t) = \int_{\Omega} e^{sx} \hat{p}(t,x) dx.$$
 (11)



22 Page 8 of 32 C. Villa et al.

We see from this definition that M(0,t) = 1 due to the scaling of $\hat{p}(t,x)$ by the total population size at all times t. The higher moments of $\hat{p}(t,x)$, where $m_k(t)$ denotes the k-th moment, are given by

$$m_k(t) = \partial_s^k M(s, t)|_{s=0}$$
 for $k \geqslant 1$. (12)

Similar to Curto and di Dio (2023), these higher moments are explicitly time dependent. As Ω is compact, it follows from the Stone-Weierstrass theorem and the solution of the Hausdorff Moment Problem that the sequence of moments, $\{m_k(t)\}_{k=1}^{\infty}$, uniquely determines the distribution $\hat{p}(t,x)$. Indeed, if Ω is not compact, as in some of our examples, then the mapping between moments and distribution is more subtle.

Using the definition (10), the ODE for the evolution of the population size P(t) in Eq. (7) becomes

$$\frac{\mathrm{d}}{\mathrm{d}t}P(t) = \left(\int_{\Omega} f(t,x)\hat{p}(t,x)\mathrm{d}x - \frac{P(t)}{\kappa}\right)P(t). \tag{13}$$

We note that P(t) thus satisfies a generalized logistic equation with growth rate and carrying capacity dependent on the phenotypic distribution $\hat{p}(t,x)$. Thus, we now focus on the evolution of $\hat{p}(t,x)$.

3.3 A system of integro-differential equations for the moments of $\hat{p}(t,x)$

Proposition 3.2 Let p(t, x) satisfy Eq. (2), along with boundary conditions (3), initial conditions (4) and definition (1). Then, the 0-th moment of $\hat{p}(t, x)$ defined in (10) is $m_0(t) = 1$ for all $t \ge 0$ and, under assumption (5), the moments $m_k(t)$ ($k \in \mathbb{N}$, $k \ge 1$) satisfy the following system of integro-differential equations

$$\frac{\mathrm{d}}{\mathrm{dt}}m_{1}(t) = \left[-\beta\left[\hat{p}(t,x)\right]\right]_{\partial\Omega} + \int_{\Omega}V(t,x)\hat{p}(t,x)\mathrm{d}x + \int_{\Omega}xf(t,x)\hat{p}(t,x)\mathrm{d}x - m_{1}(t)\int_{\Omega}f(t,x)\hat{p}(t,x)\mathrm{d}x\right],$$

$$\frac{\mathrm{d}}{\mathrm{dt}}m_{k}(t) = \beta k(k-1)m_{k-2}(t) - \beta n\left[x^{k-1}e^{xs}\hat{p}(t,x)\right]|_{\partial\Omega} + k\int_{\Omega}x^{k-1}V(x,c)\hat{p}(t,x)\mathrm{d}x$$

$$+ \int_{\Omega}x^{k}f(x,c)\hat{p}(t,x)\mathrm{d}x - m_{k}(t)\int_{\Omega}f(x,c)\hat{p}(t,x)\mathrm{d}x \qquad k \geqslant 2,$$
(14)

complemented with initial conditions

$$m_k(0) = \left(\frac{1}{\int_{\Omega} p^0(s) ds}\right) \int_{\Omega} x^k p^0(x) dx, \quad \text{for} \quad k \geqslant 1$$
 (15)

and the identity $m_{\theta}(t) = 1$ for all $t \ge \theta$.

Proof The proof of Proposition 3.2 relies on the use of the moment generating function of the distribution, introduced in Eq. (11) of Section 3.2, to derive the higher order moments.



Step 1: 0-th moment. It follows immediately from the definition of $\hat{p}(t,x)$ in Eq. (10) and the moment generating function in Eq. (11) that $m_0(t)=1$ for all time. Step 2: evolution of the moment generating function. We multiply Eq. (2) by e^{sx} and integrate with respect to x to find

$$\partial_t \left[\int_{\Omega} e^{sx} p(t, x) dx \right] - \int_{\Omega} \left(e^{sx} \partial_x \left[\beta \partial_x p(t, x) - V(t, x) p(t, x) \right] \right) dx$$
$$= \int_{\Omega} \left(f(t, x) - \frac{P(t)}{\kappa} \right) e^{sx} p(t, x) dx.$$

Multiplying the first term by unity, i.e. by P(t)/P(t), and using definition (11) yields

$$\partial_t \left[M(s,t)P(t) \right] - \int_{\Omega} \left(e^{sx} \partial_x \left[\beta \partial_x p(t,x) - V(t,x)p(t,x) \right] \right) dx$$
$$= \int_{\Omega} \left(f(t,x) - \frac{P(t)}{\kappa} \right) e^{sx} p(t,x) dx.$$

The second term on the left-hand-side can be integrated by parts twice and, after imposing boundary condition Eq. (3), this gives

$$\int_{\Omega} e^{sx} \partial_x \left[\beta \partial_x p(t, x) - V(t, x) p(t, x) \right] dx$$

$$= -s\beta \left[e^{xs} p(t, x) \right] \left| \partial_{\Omega} + \beta s^2 M(s, t) P(t) + s \int_{\Omega} e^{sx} V(t, x) p(t, x) dx.$$

Altogether this gives

$$P(t)\partial_t M(s,t) + M(s,t)\frac{\mathrm{d}}{\mathrm{d}t}P(t) = -s\beta[e^{xs}p(t,x)]|_{\partial\Omega} + \beta s^2 M(s,t)P(t)$$
$$+ s\int_{\Omega} e^{sx}V(x,c)p(t,x)\mathrm{d}x$$
$$+ \int_{\Omega} f(x,c)e^{sx}p(t,x)\mathrm{d}x - \frac{P(t)}{\kappa}M(s,t)m_0(t).$$

Substituting (7) and diving by P(t) > 0, which is non-zero as proved in Lemma 3.1, we find

$$\partial_t M(s,t) = -s\beta [e^{xs}\hat{p}(t,x)] |_{\partial\Omega} + \beta s^2 M(s,t) + s \int_{\Omega} e^{sx} V(t,x) \hat{p}(t,x) dx$$

$$+ \int_{\Omega} f(t,x) e^{sx} \hat{p}(t,x) dx - M(s,t) \int_{\Omega} f(t,x) \hat{p}(t,x) dx,$$
(16)

where we used definition (10).

Step 3: the first moment. Differentiating (16) once with respect to s gives



22 Page 10 of 32 C. Villa et al.

$$\begin{split} \partial_t [\partial_s M(s,t)] &= -\beta \left(\left[e^{xs} \hat{p}(t,x) \right] |_{\partial\Omega} + s [x e^{xs} \hat{p}(t,x)] |_{\partial\Omega} \right) + \beta \left(2s M(s,t) + s^2 \partial_s M(s,t) \right) \\ &+ \int_{\Omega} e^{sx} V(t,x) \hat{p}(t,x) \mathrm{d}x \\ &+ s \int_{\Omega} x e^{sx} V(t,x) \hat{p}(t,x) \mathrm{d}x + \int_{\Omega} x f(t,x) e^{sx} \hat{p}(t,x) \mathrm{d}x \\ &- \left[\partial_s M(s,t) \right] \int_{\Omega} f(t,x) \hat{p}(t,x) \mathrm{d}x. \end{split}$$

which, after setting s = 0, immediately gives

$$\frac{\mathrm{d}}{\mathrm{d}t} m_1(t) = -\beta \left[\hat{p}(t,x) \right] |_{\partial\Omega} + \int_{\Omega} V(t,x) \hat{p}(t,x) \mathrm{d}x$$
$$+ \int_{\Omega} x f(t,x) \hat{p}(t,x) \mathrm{d}x - m_1(t) \int_{\Omega} f(t,x) \hat{p}(t,x) \mathrm{d}x,$$

which is the first equation in Eq. (14). This is complemented with the initial condition

$$m_1(0) = \int_{\Omega} x \hat{p}(0, x) dx = \frac{1}{P(0)} \int_{\Omega} x p^0(x) dx,$$

obtained from the definition (12) and initial condition (4).

Step 4: the k-th moment. For $k \ge 2$, we calculate the k-th derivatives with respect to s of the terms on the right-hand-side of (16) to find, by induction, the following:

$$\begin{split} \partial_s^k \big[s\beta \left[e^{xs} \hat{p}(t,x) \right] \big|_{\partial\Omega} \big] = & \beta \big(k \left[x^{k-1} e^{xs} \hat{p}(t,x) \right] \big|_{\partial\Omega} + s \left[x^k e^{xs} \hat{p}(t,x) \right] \big|_{\partial\Omega} \big), \\ \partial_s^k \left[\beta s^2 M(s,t) \right] = & \beta k (k-1) \partial_s^{k-2} M(s,t) \\ & + \beta \left(2ks \partial_s^{k-1} M(s,t) + s^2 \partial_s^k M(s,t) \right), \\ \partial_s^k \left[s \int_{\Omega} e^{sx} V(x,c) \hat{p}(t,x) \mathrm{d}x \right] = & \int_{\Omega} \left(kx^{k-1} + sx^k \right) e^{sx} V(x,c) \hat{p}(t,x) \mathrm{d}x, \\ \partial_s^k \left[\int_{\Omega} e^{sx} f(x,c) \hat{p}(t,x) \mathrm{d}x \right] = & \int_{\Omega} x^k e^{sx} f(x,c) \hat{p}(t,x) \mathrm{d}x. \end{split}$$

Then, differentiating (16) k times and setting s = 0, one retrieves, for $k \ge 2$,

$$\frac{\mathrm{d}}{\mathrm{dt}} m_k(t) = -\beta k \left[x^{k-1} e^{xs} \hat{p}(t,x) \right] |_{\partial\Omega} + \beta k(k-1) m_{k-2}(t) + \int_{\Omega} n x^{k-1} V(x,c) \hat{p}(t,x) \mathrm{d}x
+ \int_{\Omega} x^k f(x,c) \hat{p}(t,x) \mathrm{d}x - m_k(t) \int_{\Omega} f(x,c) \hat{p}(t,x) \mathrm{d}x,$$
(17)

as in Eq. (14). This is complemented with the initial condition

$$m_k(0) = \int_{\Omega} x^k \hat{p}(0, x) dx = \frac{1}{P(0)} \int_{\Omega} x^k p^0(x) dx,$$



obtained, again, from the definition (12) and initial condition (4), completing (15).

Remark 3.3 The integro-differential equations for $m_k(t)$ include the distribution $\hat{p}(t,x)$ evaluated on the boundary $\partial\Omega$. Due to diffusion, the distribution is not identically zero at the boundary. However, the biological interpretation of the phenotypic variable (see Remark 2.1) implies that the population density at the boundary, while non-zero, is sufficiently small to be unobservable in biological data. Therefore, in what follows, we make the biologically motivated assumption that the contribution of the boundary terms is negligible, so

$$[\hat{p}(t,x)]|_{\partial\Omega} = [x^k \hat{p}(t,x)]|_{\partial\Omega} = 0.$$
 (18)

3.4 Restriction to a bounded phenotypic domain

The system of equations in (14) involves integrating $\hat{p}(t,x)$ over the entire phenotypic domain Ω . Consequently, without making any further assumptions on the phenotypic distribution, the system (14) is circular as the resulting integro-differential equations for the moments $m_n(t)$ a priori require the distribution $\hat{p}(t,x)$. Until now, we have considered a generic compact and connected phenotypic domain $\Omega = [l, L]$, intrinsic growth rate f(t, x), and adaptation velocity V(t, x). Importantly, the integral terms in (14) depend on these functions and implicitly on the domain Ω . Indeed, it is possible to restrict Ω to the unit interval via a simple linear transformation (Almeida et al. 2024; Stace et al. 2020).

We now show that, by considering a bounded phenotypic domain restricted to $\Omega = [0, 1]$, and functions f(t, x) and V(t, x) that are analytic in phenotype space, we can eliminate the redundancy in Eq. (14). Specifically, building on the analytical strategies adopted in Dieckmann and Law (1996); Engblom (2006); Lee et al. (2009), we show how utilizing the Taylor expansions of both f(t, x) and V(t, x) transforms Eq. (14) into a system of differential equations that depend only on the moments $m_k(t), k \geqslant 1.$

Corollary 3.4 Consider $x \in \Omega \equiv [0, 1]$. Let p(t, x) satisfy Eq. (2), along with boundary conditions (3), initial conditions (4) and definition (1). Further, assume that both f and V are analytic functions of x and that equality (18) holds.

Then, $m_0(t) = 1$ for all $t \ge 0$ by definition, and the higher order moments $m_k(t)$ $(k \ge 1)$ of the phenotypic distribution $\hat{p}(t,x)$ satisfy the following system of **ODEs**



22 Page 12 of 32 C. Villa et al.

$$\frac{d}{dt}m_{1}(t) = \sum_{n=0}^{\infty} (V_{n}(t) - m_{1}(t)f_{n}(t)) \left[\sum_{i=0}^{n} (-1)^{i} \binom{n}{i} (m_{1}(t))^{i} \right] m_{n-i}(t)
+ \sum_{n=0}^{\infty} f_{n}(t) \left[\sum_{i=0}^{n} (-1)^{i} \binom{n}{i} (m_{1}(t))^{i} m_{n+1-i}(t) \right]
\frac{d}{dt}m_{k}(t) = -m_{k}(t) \sum_{n=0}^{\infty} f_{n}(t) \left[\sum_{i=0}^{n} (-1)^{i} \binom{n}{i} (m_{1}(t))^{i} m_{n-i}(t) \right]
+ \beta k(k-1) m_{k-2}(t) + \sum_{n=0}^{\infty} \left[\sum_{i=0}^{n} (-1)^{i} \binom{n}{i} (m_{1}(t))^{i} \right]
\left[f_{n}(t) m_{n+k-i}(t) + kV_{n}(t) m_{n+(k-1)-i}(t) \right], k \ge 2.$$

with initial conditions given by Eq. (15), and where $f_n(t)$ and $V_n(t)$ are defined as

$$f_n(t) = \frac{\partial_x^n f(t, x)|_{x=m_1(t)}}{n!}$$
 and $V_n(t) = \frac{\partial_x^n V(t, x)|_{x=m_1(t)}}{n!}$. (20)

Proof As both f and V are analytic functions of x, we Taylor expand these functions about the first moment $m_1(t)$ to find

$$f(x,t) = \sum_{n=0}^{\infty} \frac{\partial_x^n f(t,x)|_{x=m_1(t)} (x - m_1(t))^n}{n!} \quad \text{and} \quad V(x,t) = \sum_{n=0}^{\infty} \frac{\partial_x^n V(x,t)|_{x=m_1(t)} (x - m_1(t))^n}{n!}.$$

Then, using definitions (20), the binomial expansion of $(x - m_1(t))^n$ gives

$$f(x,c) = \sum_{n=0}^{\infty} f_n(t) \left[\sum_{i=0}^{n} (-1)^i \binom{n}{i} x^{n-i} (m_1(t))^i \right] \text{ and }$$

$$V(x,c) = \sum_{n=0}^{\infty} V_n(t) \left[\sum_{i=0}^{n} (-1)^i \binom{n}{i} x^{n-i} (m_1(t))^i \right].$$

Thus, utilizing the Taylor expansion of f and the definition of m_n , combining (11)-(12), gives

$$\int_{0}^{1} f(x,c)\hat{p}(t,x)dx = \sum_{n=0}^{\infty} \left[\sum_{i=0}^{n} (-1)^{i} f_{n}(t) \begin{pmatrix} n \\ i \end{pmatrix} (m_{1}(t))^{i} \int_{0}^{1} x^{n-i} \hat{p}(t,x)dx \right]$$
$$= \sum_{n=0}^{\infty} \left[\sum_{i=0}^{n} (-1)^{i} f_{n}(t) \begin{pmatrix} n \\ i \end{pmatrix} (m_{1}(t))^{i} m_{n-i}(t) \right].$$



Then, for integer k, a similar calculation yields

$$\int_0^1 x^k f(x,c) \hat{p}(t,x) dx = \sum_{n=0}^{\infty} \left[\sum_{i=0}^n (-1)^i f_n(t) \begin{pmatrix} n \\ i \end{pmatrix} (m_1(t))^i m_{n+k-i}(t) \right],$$

and

$$\int_0^1 kx^{k-1} V(x,c) \hat{p}(t,x) dx = \sum_{n=0}^\infty V_n(t) \left[\sum_{i=0}^n k(-1)^i \binom{n}{i} (m_1(t))^i m_{n+(k-1)-i}(t) \right].$$

Inserting these expansions into the ODEs (14), and using (18), immediately yields Eq. (19).

These Taylor expansions replace the integral terms in (14) by weighed moments of the distribution $\hat{p}(x,t)$. However, the resulting differential equations involve moments of all orders, each of which needs to be defined by a corresponding ODE. Consequently, replacing the integral terms by the corresponding infinite summations in (14) leads to a system of infinitely many ODEs wherein the differential equation for the k-th moment depends on higher order moments. Nevertheless, higher order moments are not generally used to describe biological data. Therefore, we proceed under the modelling assumption that the phenotypic density function p(t, x), and thus \hat{p} , is sufficiently well characterised by its first N moments, so we assume that we can discard the higher order moments. We illustrate how this assumption has been applied in existing models in Sect. 4 and discuss the limitations of this assumption in the Discussion. Moreover, we consider the asymptotic behaviour of the terms in the summations, to truncate the series and close the system.

3.5 Series truncation and system closure

Consider the infinite series appearing in Eq. $(19)_1$, i.e. the term

$$T(t) = \sum_{n=0}^{\infty} f_n(t) \left[\sum_{i=0}^{n} (-1)^i \binom{n}{i} (m_1(t))^i m_{n-i}(t) \right].$$

Consider the fact that $0 < m_1(t) < 1$ for all $t \ge 0$, where the strict inequality can be ensured by appropriate modelling choices, as discussed in Remark 3.3. The strict upper bound on $m_1(t)$ implies that $(m_1)^i \to 0$ as $i \to \infty$. Having chosen f(t, x) analytic in a bounded domain, $f_n(t)$ is bounded for all $n \in \mathbb{N}$, so the coefficients of $(m_1)^i$ are bounded. We may choose $M \in \mathbb{N}$ at which to truncate the Taylor series expansions for f and V. This allows us to truncate the infinite summations at M and approximate T(t) by



22 Page 14 of 32 C. Villa et al.

$$T_M(t) = \sum_{n=0}^{M} f_n(t) \left[\sum_{i=0}^{n} (-1)^i \begin{pmatrix} n \\ i \end{pmatrix} (m_1(t))^i m_{n-i}(t) \right].$$

The same truncation can be applied to the infinite summations in Eq (19) involving V_n .

Moreover, as a result of the assumption that the phenotypic distribution $\hat{p}(t, x)$ is sufficiently well characterised by its first N moments, we find that the system (19) can be approximated by a finite system of ODEs for the N moments of $\hat{p}(t, x)$. The overall dynamics of the phenotypic density function of the population are approximated by

$$\frac{\mathrm{d}}{\mathrm{dt}}P(t) = P(t) \sum_{n=0}^{M} f_n(t) \left[\sum_{i=0}^{n} (-1)^i \binom{n}{i} (m_1(t))^i m_{n-i}(t) \right] - \frac{P^2(t)}{\kappa},$$

$$\frac{\mathrm{d}}{\mathrm{dt}}m_1(t) = \sum_{n=0}^{M} (V_n(t) - m_1(t)f_n(t)) \left[\sum_{i=0}^{n} (-1)^i \binom{n}{i} (m_1(t))^i m_{n-i}(t) \right] + \sum_{n=0}^{M} f_n(t) \left[\sum_{i=0}^{n} (-1)^i \binom{n}{i} (m_1(t))^i m_{n+1-i}(t) \right],$$

$$\frac{\mathrm{d}}{\mathrm{dt}}m_k(t) = -m_k(t) \sum_{n=0}^{M} f_n(t) \left[\sum_{i=0}^{n} (-1)^i \binom{n}{i} (m_1(t))^i m_{n-i}(t) \right] + \beta k(k-1) m_{k-2}(t)$$

$$+ k \sum_{n=0}^{M} V_n(t) \left[\sum_{i=0}^{n} (-1)^i \binom{n}{i} (m_1(t))^i m_{n+(k-1)-i}(t) \right]$$

$$+ \sum_{n=0}^{M} f_n(t) \left[\sum_{i=0}^{n} (-1)^i \binom{n}{i} (m_1(t))^i m_{n+k-i}(t) \right], \quad 2 \leqslant k \leqslant N.$$

The corresponding initial conditions of Eq. (21) are obtained directly from the initial phenotypic distribution $\hat{p}(0,x)$ via Eq. (15). While system (21) is finite, it still involves the moments m_k for k=N+1,...,N+M. To close the system one may choose, for instance, Gaussian closure by setting

$$m_k = m_1 m_{k-1} + k(m_2 - m_1^2) m_{k-2}$$
 for $k = N+1, ..., N+M$, (22)

or truncation closure by setting

$$m_k = 0 \text{ for } k = N+1, ..., N+M,$$
 (23)

- in which case system (21) reads as (32).

Other approaches to closing this system of ODEs to approximate the moments of the phenotypic distribution are possible (Browning et al. 2020; Wagner et al. 2022).



4 Special cases and examples in the literature

We here expand on some examples of how our generalised approach can be applied to more specific cases. We recover ODE systems for the moments of the phenotypic distribution previously considered in the literature from the generalised system (19), derived in Sect. 3. This procedure also brings to light the details of how the obtained systems depend on the underlying assumptions on the nature of the phenotypic distribution or specific modelling choices.

4.1 The case of f and V polynomials

We now focus on the case in which f(t, x) and V(t, x) are defined as polynomial functions of x, as in various mathematical models employing PDEs in the form of Eq. (2) for the adaptive dynamics of a phenotype-structured population of cells, e.g. see Almeida et al. (2024); Chisholm et al. (2016b) and references therein.

If the functions f and V are polynomials then, as in Curto and di Dio (2023), one need not restrict the domain to a bounded set for the results of Sect. 3 to hold. In fact, a polynomial of order $D \in \mathbb{N}$ can easily be expressed in the form of a Taylor series truncated at D, as all derivatives of order higher than D will be zero. It is then natural to replace M in the upper bounds of the summations in system (32) by $D := \max(D_f, D_V)$, where f(t, x) and V(t, x) are polynomials of order D_f and D_V , respectively. Then one need not rely on the restriction of Ω to the interval [0, 1] to ensure that the infinite summations, a product of the Taylor expansion of f and V, can be truncated at some $M \in \mathbb{N}$ which, we re-iterate, rely on the fact that $0 < m_1 < 1$ under this domain restriction. This allows the extension of the results to the case in which $\Omega = \mathbb{R}$, as considered in previous works deriving a system of ODEs for the moments of the phenotypic density function starting from phenotype-structured PDEs (Almeida et al. 2024, 2019; Ardaševa et al. 2020; Chisholm et al. 2016b; Lorenzi et al. 2015; Villa et al. 2021).

We remark that, while choosing f and V to be polynomials allows one to bypass choosing M for truncation of the infinite series, it does not automatically close the system of ODEs for the moments, and one is still required to identify the highest moment required to characterise the distribution to achieve this. Further, as $\Omega = \mathbb{R}$ is not compact, the moment sequence is not sufficient to characterise the distribution without additional assumptions. In the aforementioned papers, this was done implicitly by introducing stronger assumptions on the shape of the phenotypic distribution, which could be introduced only thanks to the use of an infinite domain.

Example from the literature: a Gaussian distribution. Consider $\Omega \equiv \mathbb{R}$, as well as f(t, x) and V(t, x) defined by

$$f(t,x) = a(t) - b(t) (x - X(t))^{2}$$
 and $V(t,x) \equiv V_{0}(t)$, (24)

i.e. polynomials of order 2 and 0, respectively. In definition (24) for f, X(t) models the fittest phenotypic trait, a(t) the associated maximal background fitness and b(t) is a nonlinear selection gradient measuring the strength of the selective environment. Under the assumption of an initial phenotypic distribution $p^0(x)$ in a Gaussian form,



Chisholm et al. (2016b) first showed that p(t, x) maintains a Gaussian form at all times, with the population size P(t), the mean $m_1(t)$ and variance $\sigma^2(t)$ of the distribution satisfying the system of ODEs

$$\frac{\mathrm{d}}{\mathrm{dt}}P(t) = \left[a(t) - b(t) \left(m_1(t) - X(t)\right)^2 - b(t)\sigma^2(t)\right] P(t) - \frac{P^2(t)}{\kappa},
\frac{\mathrm{d}}{\mathrm{dt}}m_1(t) = -2b(t) \left(m_1(t) - X(t)\right)\sigma^2(t) + V_0(t),
\frac{\mathrm{d}}{\mathrm{dt}}\sigma^2(t) = 2\beta - 2b\sigma^4(t),$$
(25)

complemented with initial conditions P(0), $m_1(0)$ and $\sigma^2(0)$, i.e. the corresponding moments characterising the initial Gaussian phenotypic density function $p^0(x)$. Analogous assumptions and results have since appeared in several following works by Lorenzi and coworkers (Almeida et al. 2024, 2019; Ardaševa et al. 2020; Lorenzi et al. 2015; Villa et al. 2021) modelling cancer adaptive dynamics in different settings. System (25) can be obtained via formal calculations following the substitution of a Gaussian ansatz in Eq. (2) under definitions (24), with most publications working with the inverse variance $v=(\sigma^2)^{-1}$ for convenience.

Retrieving system (25) from our generalised approach. Now consider the case in which f and V are defined as in (24). We show how the example above is a sub-case of our generalised approach, assuming that the phenotypic distribution can be fully characterised by its first 2 moments. We thus consider system (21) with N=2, the infinite summations including $f_n(t)$ truncated at $D_f=2$ and those only including $V_n(t)$ truncated at $D_V=0$. We then choose to apply Gaussian closure—indeed the obvious choice in this case—and complement the ODE system with (22) for m_3 and m_4 . The resulting system of ODEs is

$$\frac{\mathrm{d}}{\mathrm{d}t}P(t) = P(t)\left[f_0(t) + f_2(t)(m_2 - m_1^2)\right] - \frac{P^2(t)}{\kappa},$$

$$\frac{\mathrm{d}}{\mathrm{d}t}m_1(t) = f_1(t)(m_2 - m_1^2) + V_0(t),$$

$$\frac{\mathrm{d}}{\mathrm{d}t}m_2(t) = 2V_0m_1 + 2\beta + 2f_1(t)m_1(m_2 - m_1^2) + 2f_2(t)(m_2 - m_1^2)^2,$$

which is equivalent to system (25)— this is easy to check by substituting $m_2 = \sigma^2 + m_1^2$, from the definition of second central moment, and applying the definitions of f_i (i = 0, 1, 2) and V_0 in (20) on f and V chosen in (24).

This demonstrates that system (21) may provide a good approximation for the moment dynamics of Eq. (2). We stress that in this case the systems are equivalent only thanks to the fact that f and V are polynomials of order at most 2, and the properties (22) of a Normal distribution, which may be exploited when adopting a Gaussian closure. Unlike in Almeida et al. (2024, 2019); Ardaševa et al. (2020); Chisholm et al. (2016b); Lorenzi et al. (2015); Villa et al. (2021), our procedure does not need to rely on an ansatz or an infinite domain, but it holds for the more realistic case of $\Omega = [l, L]$ and under more general assumptions on the nature of the phenotypic distribution.



4.2 An example for f and V smooth but not polynomial

For f and V polynomials, the truncation of the infinite summations in system (21) is automatic. While polynomial definitions for f and V are widely used in continuously structured models in mathematical oncology, other modelling choices may lead to alternative definitions of these functions. In general, these functions are usually sufficiently smooth to admit a Taylor series approximation (Celora et al. 2021; Cho and Levy 2018b). We now consider an example with f and V not polynomial, in which case they must be approximated by their Taylor expansions truncated at some M. Let f and V be defined as

$$f(t,x) = f_{max} \frac{x}{k_x + x} \quad \text{and} \quad V(t,x) = V_{max} \tanh(x^{\omega}) \tanh(1 - x). \quad (26)$$

This definition for f may be used in the case where x models the level of expression of some protein on the cell membrane that is required to transport nutrients into the cell, e.g. see Almeida et al. (2024), in which case a Hill function is natural following Michaelis-Menten kinetics. Then $k_x > 0$ is the Michaelis coefficient and $f_{max} \ge 0$ the maximum intrinsic growth rate. Definition (26) for V was taken from Celora et al. (2021), one of the most complex choices of V currently found in the literature, proposed following phenomenological rules to capture the effect of radiotherapy on differentiation, with $V_{max} \ge 0$ and $\omega \in \{1, 2\}$. For simplicity, we take the initial phenotypic distribution to be a truncated Normal distribution in the interval $\Omega = [l, L]$, i.e. we take

$$p(0,x) = P(0) \frac{\exp\left[-\frac{(x-\bar{x}_0)^2}{2\sigma_0^2}\right]}{\int_l^L \exp\left[-\frac{(s-\bar{x}_0)^2}{2\sigma_0^2}\right] ds}.$$
 (27)

The first step in the application of system (21) to approximate the moment dynamics is to carefully select the domain bounds, to ensure that (18) is satisfied. In Celora et al. (2021) the authors select $x \in [0,1]$ but under definition (26) for V we expect the mass to concentrate around x=1 over time and thus a wider domain is necessary. Here we use a parameter set for which the interval [l, L] = [0, 1.2] is sufficiently large—with β and σ_0^2 sufficiently small and \bar{x}_0 sufficiently far from these boundaries. We thus apply the transformation $x \to x/L$ prior to solving the ODE system numerically, to ensure that $0 < m_1(t) < 1$ for all $t \ge 0$ as required in Sect. 3.5. The results of numerical simulations shown in Fig. 1 (as well as Figs. 3 and 4 in the Supplemental Information) have been rescaled back to the original domain (by means of $m_k \to m_k \times L^k$).

Setting $\omega = 1$ in the definition (26) for V, we see in Fig. 1 that the ODE system (21) under Gaussian closure (22) provides a really good approximation of the dynamics of the moments of the phenotypic density function satisfying PDE (2) for many combinations of N and M, without needing to consider N and M particularly large. In fact, it is interesting to notice from the zoomed in insets that the best approximation—among those tested—is obtained when selecting N=2 and M=2 rather than for higher values of N and M (c.f. N=2 and M=3, or N=3 and M=1).



22 Page 18 of 32 C. Villa et al.

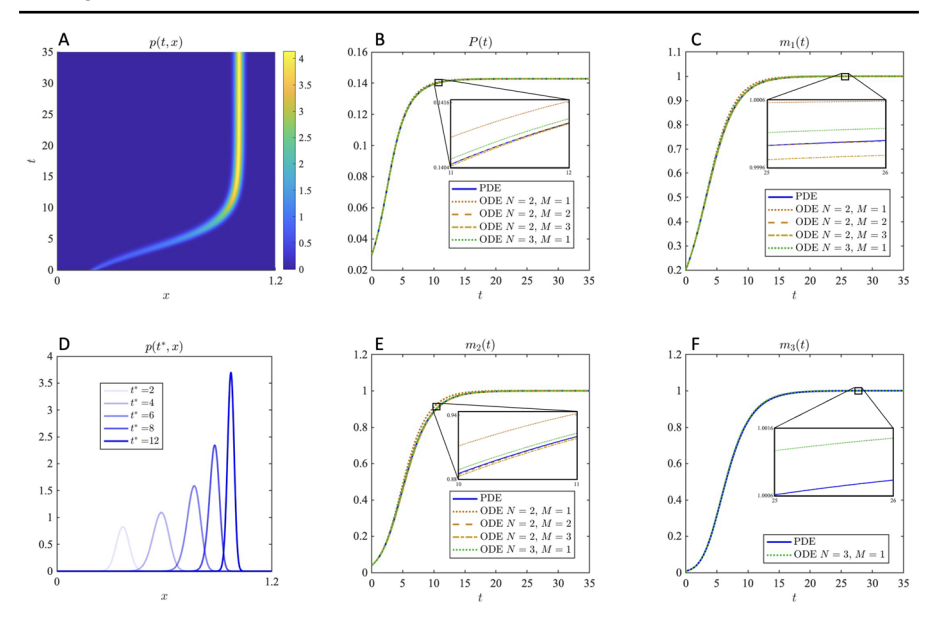


Fig. 1 Comparison between the numerical solution of PDE (2), complemented with Eq. (1) and boundary conditions (3), and that of the ODE system (21) under Gaussian closure (22), for f and V defined in (26) ($\omega=1$) and initial condition (27). The phenotypic density function p(t,x) obtained by solving the PDE is shown in the first column for $t\in[0,35]$ (panel A) and at selected times $t^*=2,4,6,8,12$ (D). The corresponding moments are plotted with a blue solid line in the remaining panels: the populations size P(t) (B), the first moment $m_1(t)$ (C), the second moment $m_2(t)$ (E) and the third moment $m_3(t)$ (F). The moments obtained from the ODE system are also shown in each panel under different choices of N and M: N=2 and M=1 (brown dotted line), N=2 and M=2 (brown dashed line), N=3 and M=1 (green dotted line). Zoomed-in sets are provided to facilitate comparison among approximations. The results correspond to the parameter set: $f_{max}=2$, $k_m=0.4$, $V_{max}=0.5$, $\omega=1$, $\kappa=0.1$, $\beta=10^{-4}$, $\bar{x}_0=0.2$, $\sigma_0=0.02$, l=0, L=1.2. The numerical schemes rely on a first order forward difference approximation for the time derivatives, second order central difference for the diffusion term and first order upwind for the advection term

As expected when looking at the solution of the PDE (cf. first column in Fig. 1), truncation closure does not perform as well as Gaussian closure (see also Fig. 3 in the Supplemental Information). In the more complex case of $\omega=2$, for which we observe a higher skewedness of the phenotypic distribution at intermediate times, not all choices of N and M provide as good an approximation (see also Fig. 4 in the Supplemental Information). Nevertheless, the observation that N=2 and M=2 yields the best approximation among those tested holds also in this case, where we also tested N=3 and M=3. Ultimately, we expect the combination of N and M that best approximate the moment dynamics to vary with the definitions of f and f0, as well as the best choice of closure for system (21). Indeed the presence of a linear diffusion term in PDE (2) may favour Gaussian-like features.



4.3 Link with canonical model of adaptive dynamics

We have seen how our model reduction procedure may perform well for nonpolynomial, but sufficiently smooth, functions f and V. Models of adaptive dynamics (Dieckmann and Law 1996; Vincent and Gatenby 2008), which model the size and mean trait of the population via two ODEs, typically utilize the "G function" formalization (Coggan and Page 2022). This "G function" links the population fitness to the phenotypic evolution by assuming that the population evolves to maximize the population fitness. In general, these adaptive dynamics models do not restrict the phenotype space Ω , but rather implicitly assume that the functions f and V are only weakly non-linear and that the population is monomorphic so that higher order moments are negligible (Dieckmann and Law 1996). In practice, this corresponds to setting M=N=1 in Sect. 3.5, and neglecting terms involving m_k, m_1^k, f_k or V_k for $k \ge 2$. These assumptions are possibly quite strong when considering cancer evolution (Aguadé-Gorgorió and Solé 2018), particularly due to the role of phenotypic diversity in the population-level response to therapy. Here, we utilize the model proposed by Pressley et al. (2021) to illustrate the possible consequences of these modelling assumptions.

4.3.1 Application to adaptive dynamics in cancer

In recent work, Pressley et al. (2021) developed a mathematical framework to capture continuous adaptation to treatment, in which the cellular phenotype is considered as a direct measure of cell resistance to anti-cancer therapy. The authors consider a monomorphic population with population size P(t) and phenotype $m_1(t)$ where we use this notation as the phenotype of a monomorphic population corresponds to the mean phenotypic state (i.e. the first moment) of a very sharp (Dirac delta) phenotypic distribution. Their model is given by

$$\frac{d}{dt}P(t) = P(t)G(m_1(t), P(t)),
\frac{d}{dt}m_1(t) = \alpha \partial_x G(x, y)|_{(x,y)=(m_1(t), P(t))}.$$
(28)

In Eq. (28), α is the speed of phenotypic adaptation and the function G captures the net proliferation rate of the population P in the presence of anti-cancer treatment under the assumption that all tumour cells have phenotype m_1 . Specifically, Pressley et al. (2021) set

$$G(m_1(t),P(t))=r(m_1(t))\left(1-\frac{P(t)}{\kappa}\right)-d-\frac{c(t)}{k+bm_1(t)}$$

where κ is the carrying capacity of the population, d is an intrinsic death rate in the absence of treatment, and



$$c(t) = \begin{cases} 1 & \text{during treatment,} \\ 0 & \text{otherwise,} \end{cases}$$

models the anti-cancer treatment. The treatment effect is modulated by the treatment resistance of the population with mean phenotype $m_1(t)$. The magnitude of the resistance benefit is modelled by b and treatment resistance has a half-effect value of k. Pressley et al. (2021) used this model to quantify the benefits of adaptive therapy. They applied treatment until the tumour reached half the initial size, P(t) = P(0)/2. Treatment was then interrupted and withheld until the tumour reached the initial size, P(t) = P(0), at which point treatment was re-applied. The model includes the cost of resistance by decreasing the intrinsic growth rate $r(m_1(t))$ of a population with mean phenotype $m_1(t)$ by

$$r(m_1(t)) = r_{max} \exp(-gm_1(t)),$$

where r_{max} is the maximal growth rate and g is the cost of resistance.

We now show how our framework can extend Eq. (28) to include population heterogeneity by considering higher order moments and setting N=M=2 in Eq. (21). Pressley et al. (2021) assume that the mean phenotype changes with direction determined by the gradient of G and scaled by an adaptation speed α . Under these assumptions, the velocity $V(t, m_1)$ in the advection term of Eq. (2) is given by

$$V(t, m_1) = \alpha \partial_x G(m_1, P). \tag{29}$$

This assumption on the velocity of the advection term represents gradient ascent toward the phenotype of optimal fitness. For notational simplicity, we write for $k \in \mathbb{N}$

$$\partial_x G(m_1, P) = \partial_x G(x, y)|_{(x,y) = (m_1(t), P(t))}$$
 and $\partial_x^k G(m_1, P) = \partial_x^k G(x, y)|_{(x,y) = (m_1(t), P(t))}$.

We emphasize that this definition of $V(t,m_1)$ follows from the modelling assumptions made by Pressley et al. (2021). However, our approximation framework applies in general to other choices for V and f. Taking N=M=2- motivated by the results of Sect. 4.2– in system (21) and using Gaussian closure, we obtain



$$\frac{\mathrm{d}}{\mathrm{dt}}P = P\left[G(m_{1}, P) + \frac{\partial_{x}^{2}G(m_{1}, P)}{2}\left(m_{2} - m_{1}^{2}\right)\right],$$

$$\frac{\mathrm{d}}{\mathrm{dt}}m_{1} = \left(\alpha + \left(m_{2} - m_{1}^{2}\right)\right)\partial_{x}G(m_{1}, P)$$

$$+ \left[\frac{\alpha}{2}\partial_{x}^{3}G(m_{1}, P) - m_{1}\frac{\partial_{x}^{2}G(m_{1}, P)}{2}\right]\left(m_{2} - m_{1}^{2}\right) + \frac{\partial_{x}^{3}G(m_{1}, P)}{6}m_{3},$$

$$\frac{\mathrm{d}}{\mathrm{dt}}m_{2} = 2\left[\alpha\partial_{x}G(m_{1}, P)m_{1}$$

$$+\alpha\partial_{x}^{2}G(m_{1}, P)\left(m_{2} - m_{1}^{2}\right) + \frac{\alpha}{2}\partial_{x}^{3}G(m_{1}, P)\left(m_{3} - 2m_{1}m_{2} + m_{1}^{3}\right)\right]$$

$$2\beta - m_{2}\left[\frac{\partial_{x}^{2}G(m_{1}, P)}{2}\left(m_{2} - m_{1}^{2}\right)\right]$$

$$+\partial_{x}G(m_{1}, P)\left(m_{3} - m_{1}m_{2}\right) + \frac{\partial_{x}^{2}G(m_{1}, P)}{2}\left(m_{4} - 2m_{1}m_{3} + (m_{1}^{2})m_{2}\right).$$

where we do not explicitly show the time-dependence of the moments to simplify the notation. Similarly, we take N=M=2 and use truncation closure to find

$$\frac{\mathrm{d}}{\mathrm{dt}}P = P\left[G(m_{1}, P) + \frac{\partial_{x}^{2}G(m_{1}, P)}{2} \left(m_{2} - m_{1}^{2}\right)\right],$$

$$\frac{\mathrm{d}}{\mathrm{dt}}m_{1} = \left(\alpha + m_{2} - m_{1}^{2}\right)\partial_{x}G(m_{1}, P)$$

$$+ \left[\alpha \frac{\partial_{x}^{3}G(m_{1}, P)}{2} - 3m_{1}(t)\frac{\partial_{x}^{2}G(m_{1}, P)}{2}\right]\left(m_{2} - m_{1}^{2}\right),$$

$$\frac{\mathrm{d}}{\mathrm{dt}}m_{2} = 2\beta + 2\alpha\partial_{x}G(m_{1}, P)m_{1} - G(m_{1}, P)m_{2}$$

$$+ \left[2\alpha\partial_{x}^{2}G(m_{1}, P) - m_{2}\frac{\partial_{x}^{2}G(m_{1}, P)}{2}\right]\left(m_{2} - m_{1}^{2}\right).$$
(31)

In both Eqs. (30) and (31), the population growth rate now depends not only on the fitness of the mean phenotype, $G(m_1, P)$, but also on it's curvature and the variance of the population about the mean phenotype, $\sigma^2 = m_2 - m_1^2$. Further, the differential equation for $m_1(t)$ links the phenotypic evolution with σ^2 in a similar manner to Dieckmann and Law (1996) in the context of genetic mutation.

To illustrate the impact of including phenotypic heterogeneity, we simulated the adaptive therapy regimen in Eqs. (28), (30) and (31). We set $\alpha=0.0001$ and otherwise used the same parameter values and initial conditions as Pressley et al. (2021), with P(0)=6000 and $m_1(0)=0$. In Eq. (30) and Eq. (31), we set $m_2(0)=m_1(0)^2$ to represent an initially monomorphic population, and set $\beta=0.0002$. In Panels A and B of Fig. 2, we show the predicted tumour population during adaptive therapy. Eq. (28) predicts long-term tumour control, with the Time-To-Progression– i.e. the first time $t=t_{TTP}$ at which $P(t_{TTP})=0.7\kappa$ – of at least 800 days. Conversely, the models that include population heterogeneity, i.e. Eqs. (30) and (31), both predict the evolution of treatment resistance and failure of adaptive therapy within 28 days. In Panel C of Fig. 2, we show the cumulative dose during adaptive treatment, which highlights the development of resistance predicted by both Eqs. (30) and (31). This



22 Page 22 of 32 C. Villa et al.

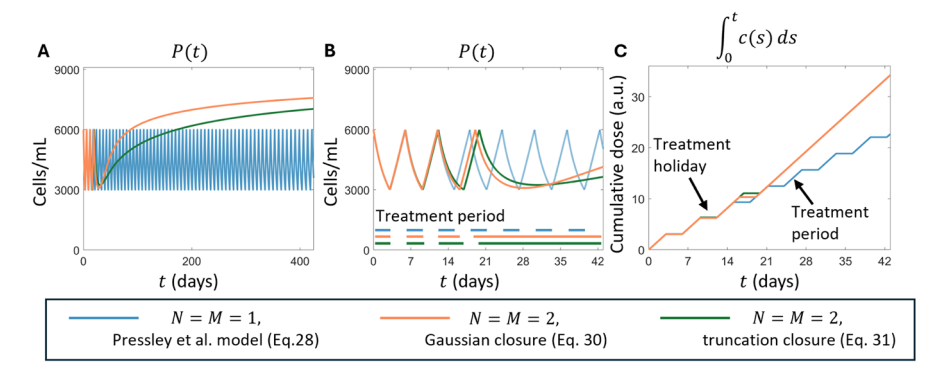


Fig. 2 Population heterogeneity drives treatment resistance in the adaptive dynamics model implemented by Pressley et al. (2021). Panels **A** and **B** show the dynamics of the simulated tumour population with and without heterogeneity. The horizontal lines in Panel B show when treatment is applied. Panel **C** shows the cumulative dose administered during the adaptive therapy treatment for each simulation. In all cases, the N=M=1 approximation, corresponding to the Pressley model in Eq. (28), is shown in blue while the orange and green curves show the N=M=2 approximation models with Gaussian and truncation closures, i.e. the models given by Eqs. (30) and (31) respectively. Other than the adaptation speed, $\alpha=0.00001$, and diffusion coefficient $\beta=0.00002$, all simulations used the parameter values given in Pressley et al. (2021)

highlights that population diversity may accelerate the development of treatment resistance as has been observed in many experimental (Bódi et al. 2017; McGranahan and Swanton 2017; Sottoriva et al. 2013; Marine et al. 2020; Craig et al. 2019) and theoretical (Almeida et al. 2019; Ardaševa et al. 2020; Lorenzi et al. 2015; Villa et al. 2021; Köhn-Luque et al. 2023; Cassidy and Humphries 2019; Lavi et al. 2013; Greene et al. 2014; Nichol et al. 2016) studies. We emphasize that the parameters used in this simulation were not obtained by fitting the model to data, but rather chosen to qualitatively illustrate the influence of including population heterogeneity in a model of adaptive evolution of treatment resistance.

5 Discussion

Mathematical models have become increasingly important in our understanding of the mechanisms driving cancer evolutionary dynamics and the role of intratumour phenotypic heterogeneity. Phenotype-structured PDE models describe the temporal dynamics of both the tumour size and phenotypic composition. In the context of adaptive dynamics in continuously structured phenotype space, these PDE models carry a distinct advantage in that individual model terms are directly biologically interpretable.

Benefits of reducing a phenotype-structured PDE to a system of ODEs. While phenotype-structured PDE models are well-poised to interpret biological data, they carry, by their very nature, challenges that do not apply to the ODE models that are routine in the interpretation of data. For example, for a mathematical model to be uniquely parameterised it must be *identifiable* (Bellman and Åström 1970; Raue et al. 2009; Cassidy 2023). Outside of recent work (Browning et al. 2024; Boiger



et al. 2016; Stapor et al. 2018), most computational tools for parameter identifiability analysis are developed for ODE models (Bellman and Åström 1970; Raue et al. 2009). Therefore, assessing parameter identifiability in PDE models often requires an ODE surrogate such as an equivalent or approximate system of moment equations (Browning et al. 2020). Parameter identifiability is particularly pertinent in the case of phenotype-structured PDE models, as determining the phenotypic distribution of a tumour sample is experimentally demanding (Brestoff and Frater 2022; Pigliucci 2010). Furthermore, numerical methods for phenotype-structured PDEs are not widely implemented in existing scientific software (Carpenter et al. 2017). Consequently, fitting these PDE models to experimental data often requires the development of problem specific software. The resulting numerical methods are typically more computationally expensive than for ODE models. As parameter estimation typically involves many simulations of the mathematical model which amplifies the increased computational cost of solving the PDE. Therefore, the ability to reduce a phenotype-structured PDE to a system of ODEs while maintaining the ability to characterise the tumour composition allows for significant computational efficiency. Summary and novelty of our model-reduction procedure. Accordingly, we proposed a generalised method to reduce a phenotype-structured PDE model of cancer adaptive dynamics to a system of ODEs for the moments of the phenotypic distribution, up to an arbitrary number of moments. This reduction allows modellers to use existing technical tools for ODE models while maintaining the biological relevance and the interpretability of the phenotype-structured PDE. The model-reduction procedure we propose relies on the use of the moment generating function of the phenotypic distribution, a Taylor series expansion of the phenotypic drift and proliferation rate functions, and truncation closure. Our work extends the analysis of Almeida et al. (2019) and Chisholm et al. (2016b), to a more biologically relevant phenotypic domain and a model without any a priori assumptions on the shape of the distribution or the dependency of the phenotypic drift and proliferation rate on the phenotypic trait. Our work also extends the analysis of Dieckmann and Law (1996) that ties a stochastic model of mutation-selection dynamics to the adaptive dynamics models in Section 4.3. Here, we have used both truncation and Gaussian closures for the resulting system of ODEs describing the moments of the phenotypic distribution \hat{p} . However, other approaches are possible and evaluating these alternative closures is an obvious area for future research.

Strengths and limitations. Our model reduction procedure is independent of both the shape of the phenotypic distribution and the functional form of the terms that characterise adaptation. This generality and flexibility lends our analysis suitable for adaptation in a wide range of contexts, both within mathematical oncology and more broadly. We expect many of the advantages conferred by the reduced model to become even more pertinent in high-dimensional phenotype spaces, particularly in the context of mechanistic interpretation of correspondingly high-dimensional multiomics data. The necessity to impose a system closure yields an approximation of the underlying dynamics. However, we highlight that the presented approach can be applied up to an arbitrary order. The question of how many moments a problem requires, the closure to apply, or the effect of closure on parameter identifiability, remains open even in fields where moment closures have a long history (Smith et al.



2007; Kuehn 2016; Ghusinga et al. 2017; Schnoerr et al. 2017; Browning et al. 2020; Wagner et al. 2022). We expect unimodal phenotypic distributions to be well characterised by lower-order moments. For high-dimensional problems, the question of closure type and order is likely determined by computational cost. Ultimately, we provide a general and flexible framework for describing adaptation in a continuously-distributed phenotype space whilst retaining the computational and analytical advantages of ODE-based approaches.

Consequences and perspectives in cancer adaptive therapy. Our work relaxes the assumptions of near-linear growth rates or vanishing variance underlying the canonical equation of adaptive dynamics (Dieckmann and Law 1996) by explicitly linking the higher-order moments of the population distribution in phenotype space with the resulting impacts on population growth and adaptation. To illustrate the possible effects of including population heterogeneity, we considered the model of adaptive dynamics in response to adaptive therapy by Pressley et al. (2021). We show that including phenotypic heterogeneity in the Pressley et al. (2021) model can lead to failure of an adaptive therapy strategy that would otherwise result in long-term tumour control. While this result is unsurprising (Bódi et al. 2017), it illustrates how phenotypic heterogeneity can drive treatment resistance (Aguadé-Gorgorió and Solé 2018; Hanahan 2022). Consequently, our results illustrate a simple way to introduce population heterogeneity in ODE models investigating the development of treatment resistance, and importance in the emergent model dynamics

In this context, our work is directly relevant to recent multi-omics-level experiments characterising cellular phenotypes. However, these high dimensional data sets are challenging to interpret and thus numerous dimensionality reduction methods have been proposed (Oshternian et al. 2024; Burkhardt et al. 2022). Amongst these are phenotype classification methods that summarise these data sets with a selected number of moments (Vogelstein et al. 2021; Tang et al. 2010). As such, momentbased descriptions are increasingly considered to describe phenotypic states and our modelling therefore offers a direct link with these emerging clinically relevant data sets. For example, bulk and single-cell sequencing have both identified continuous phenotypic adaptation in response to treatments in patient-derived xenografts carrying the BRAFV600E mutation (Xue et al. 2017). Köhn-Luque et al. (2023) have shown how to use *in vitro* dose-response experiments to parameterize mathematical models of phenotypically distinct sub-populations through the *PhenoPop* method, corresponding to a discrete phenotype distribution. The resulting models capture the sub-population dynamics but assume that each sub-population is homogeneous. Our results complement this approach by allowing for the *PhenoPop* method to also describe the population heterogeneity.



Consequently, the framework derived in this work could facilitate both the development of mathematical models and the calibration of these models by multi-omics data to understand how phenotypic heterogeneity drives the evolution of treatment resistance to targeted therapies.

Proof of Proposition 3.1

Integrating Eq. (2) with respect to x over Ω , and interchanging integration and differentiation, gives

$$\frac{\mathrm{d}}{\mathrm{d}t}P(t) = \int_{\Omega} \partial_x [\beta \partial_x p(t,x) - V(t,x)p(t,x)] \mathrm{d}x + \int_{\Omega} \left(f(t,x) - \frac{P(t)}{\kappa} \right) p(t,x) \mathrm{d}x,$$

where we have also used definition (1). Applying the boundary condition (3), and again using (1), immediately gives Eq. (7). The initial condition (8) can be obtained by integrating the initial condition (4) directly. The strict positivity of P(0) follows directly from the assumption imposed on $p^0(x)$ in (4). Under assumption (6), from Eq. (7) the following inequality holds

$$\frac{\mathrm{d}}{\mathrm{d}t}P(t) \leqslant f_{\mathrm{M}} \int_{\Omega} p(t,x) \mathrm{d}x - \frac{P^{2}(t)}{\kappa} \leqslant \left(f_{\mathrm{M}} - \frac{P(t)}{\kappa}\right) P(t),$$

which, setting $\overline{P} := \max(P(0), f_{M}\kappa)$, gives the upper bound in (9). Similarly, we have

$$\frac{\mathrm{d}}{\mathrm{d}t}P(t) \geqslant f_{\mathrm{m}} \int_{\Omega} p(t,x) \mathrm{d}x - \frac{P^{2}(t)}{\kappa} \geqslant \left(f_{\mathrm{m}} - \frac{P(t)}{\kappa}\right) P(t).$$

We note that the lower bound for $\frac{d}{dt}P(t)$ is a scalar logisitic differential equation. Thus, Gronwall's inequality immediately yields the strict positivity of P(t) for all t > 0.

Full system under truncation closure

System (21) under truncation closure (23) can be rewritten as



22 Page 26 of 32 C. Villa et al.

$$\frac{\mathrm{d}}{\mathrm{dt}}P(t) = P(t) \sum_{n=0}^{M} f_n(t) \left[\sum_{i=\max(0,n-N)}^{n} (-1)^i \binom{n}{i} (m_1(t))^i m_{n-i}(t) \right] - \frac{P^2(t)}{\kappa},$$

$$\frac{\mathrm{d}}{\mathrm{dt}}m_1(t) = \sum_{n=0}^{M} (V_n(t) - m_1(t)f_n(t)) \left[\sum_{i=\max(0,n-N)}^{n} (-1)^i \binom{n}{i} (m_1(t))^i m_{n-i}(t) \right] + \sum_{n=0}^{M} f_n(t) \left[\sum_{i=\max(0,n+1-N)}^{n} (-1)^i \binom{n}{i} (m_1(t))^i m_{n+1-i}(t) \right],$$

$$\frac{\mathrm{d}}{\mathrm{dt}}m_k(t) = -m_k(t) \sum_{n=0}^{M} f_n(t) \left[\sum_{i=\max(0,n-N)}^{n} (-1)^i \binom{n}{i} (m_1(t))^i m_{n-i}(t) \right] + \beta k(k-1) m_{k-2}(t)$$

$$+ k \sum_{n=0}^{M} V_n(t) \left[\sum_{i=\max(0,n+(k-1)-N)}^{n} (-1)^i \binom{n}{i} (m_1(t))^i m_{n+(k-1)-i}(t) \right]$$

$$+ \sum_{n=0}^{M} f_n(t) \left[\sum_{i=\max(0,n+(k-1)-N)}^{n} (-1)^i \binom{n}{i} (m_1(t))^i m_{n+k-i}(t) \right], \quad 2 \leq k \leq N.$$

Supplementary figures

See Figs. 3 and 4.

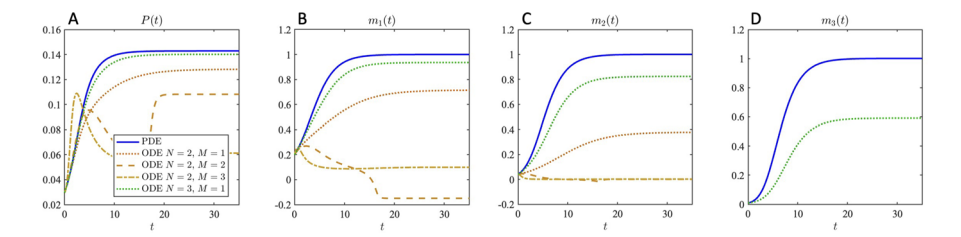


Fig. 3 Comparison between the numerical solution of PDE (2), complemented with Eq. (1) and boundary conditions (3), and that of the ODE system (21) under truncation closure (23), for f and V defined in (26) ($\omega=2$) and initial condition (27). The moments corresponding to the phenotypic density function p(t,x) obtained solving the PDE are plot with a blue solid line: the populations size P(t) (panel A), the first moment $m_1(t)$ (B), the second moment $m_2(t)$ (C) and the third moment $m_3(t)$ (D). The moments obtained from the ODE system are also shown in each panel under different choices of N and M: N=2 and M=1 (brown dotted line), N=2 and M=2 (brown dashed line), N=2 and M=3 (brown dash-dotted line), N=3 and M=1 (green dotted line), N=3 and M=1 (green dashed line). The results correspond to the parameter set: $f_{max}=2$, $f_{max}=0.4$, $f_{max}=0.5$, f_{max}



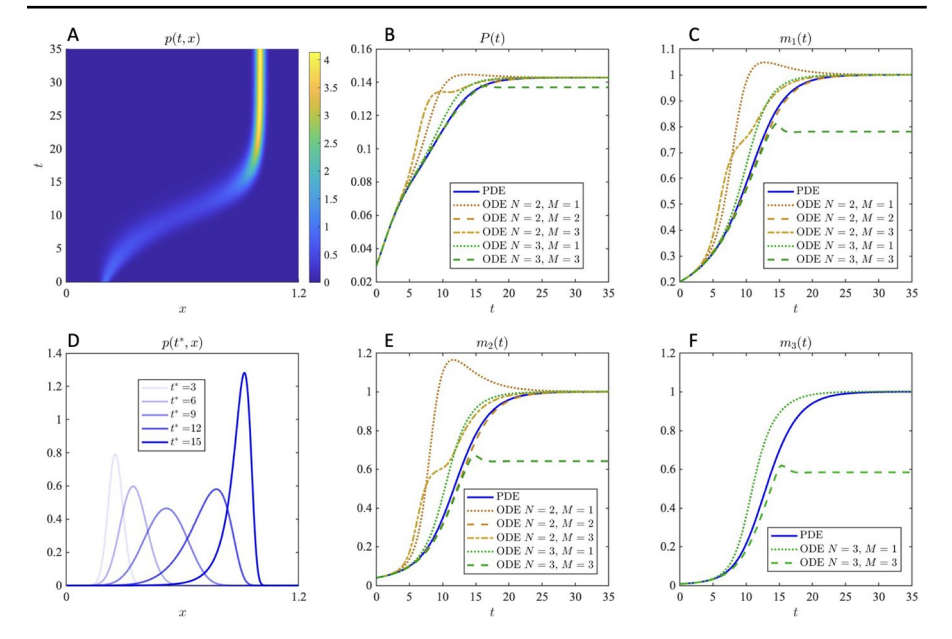


Fig. 4 Comparison between the numerical solution of PDE (2), complemented with Eq. (1) and boundary conditions (3), and that of the ODE system (21) under Gaussian closure (22), for f and V defined in (26) ($\omega=2$) and initial condition (27). The phenotypic density function p(t,x) obtained solving the PDE is shown in the first column for $t\in[0,35]$ (panel A) and at selected times $t^*=3,6,9,12,15$ (D). The corresponding moments are plot with a blue solid line in the remaining panels: the populations size P(t) (B), the first moment $m_1(t)$ (C), the second moment $m_2(t)$ (E) and the third moment $m_3(t)$ (F). The moments obtained from the ODE system are also shown in each panel under different choices of N and M: N=2 and M=1 (brown dotted line), N=2 and M=2 (brown dashed line), N=3 and M=1 (green dotted line), N=3 and M=1 (green dashed line). The results correspond to the parameter set: $f_{max}=2$, $f_{max}=0.4$, $f_{max}=0.5$

Acknowledgements This work was partially supported by a Heilbronn Institute for Mathematical Research Small Maths Grant to TC. APB thanks the Mathematical Institute, Oxford for a Hooke Research Fellowship. ALJ thanks the London Mathematical Society. SH was funded by Wenner-Gren Stiftelserna/ the Wenner-Gren Foundations (WGF2022-0044) and the Kjell och Märta Beijer Foundation. This project was partially supported by the European Union's Horizon 2020 research and innovation programme under the Marie Skłodowska-Curie grant agreement No 945298-ParisRegionFP. CV is a Fellow of the Paris Region Fellowship Programme, supported by the Paris Region.

Code availability The Matlab code underlying the simulations in Section 4.2 (which allows to test the approximation for custom f and V for various N and M) is available at https://github.com/ChiaraVilla/Villa 2025Reducing, while the code underlying the simulations in Section 4.3 is available at https://github.com/ttcassid//Phenotype_Continuous_Adaptation.

Declarations

Conflict of interest No potential conflict of interest to declare.



Open Access This article is licensed under a Creative Commons Attribution 4.0 International License, which permits use, sharing, adaptation, distribution and reproduction in any medium or format, as long as you give appropriate credit to the original author(s) and the source, provide a link to the Creative Commons licence, and indicate if changes were made. The images or other third party material in this article are included in the article's Creative Commons licence, unless indicated otherwise in a credit line to the material. If material is not included in the article's Creative Commons licence and your intended use is not permitted by statutory regulation or exceeds the permitted use, you will need to obtain permission directly from the copyright holder. To view a copy of this licence, visit http://creativecommons.org/licenses/by/4.0/.

References

- Aguadé-Gorgorió G, Solé R (2018) Adaptive dynamics of unstable cancer populations: the canonical equation. Evol Appl 11(8):1283–1292
- Almeida L, Bagnerini P, Fabrini G, Hughes BD, Lorenzi T (2019) Evolution of cancer cell populations under cytotoxic therapy and treatment optimisation: insight from a phenotype-structured model. ESAIM Math Model Num 53(4):1157–1190
- Almeida L, Denis JA, Ferrand N, Lorenzi T, Prunet A, Sabbah M, Villa C (2024) Evolutionary dynamics of glucose-deprived cancer cells: insights from experimentally informed mathematical modelling. J R Soc Interface 21(210):20230587
- Altrock PM, Liu LL, Michor F (2015) The mathematics of cancer: integrating quantitative models. Nat Rev Cancer 15(12):730–745
- Anderson AR, Weaver AM, Cummings PT, Quaranta V (2006) Tumor Morphology and Phenotypic Evolution Driven by Selective Pressure from the Microenvironment. Cell 127(5):905–915
- Ardaševa A, Gatenby RA, Anderson AR, Byrne HM, Maini PK, Lorenzi T (2020) Evolutionary dynamics of competing phenotype-structured populations in periodically fluctuating environments. J Math Biol 80:775–807
- Bell CC, Gilan O (2020) Principles and mechanisms of non-genetic resistance in cancer. Br J Cancer 122(4):465–472
- Bellman R, Åström K (1970) On structural identifiability. Math Biosci 7(3-4):329-339
- Bódi Z, Farkas Z, Nevozhay D, Kalapis D, Lázár V, Csörgö B, Nyerges Á, Szamecz B, Fekete G, Papp B, Araújo H, Oliveira JL, Moura G, Santos MAS, Székely T Jr, Balázsi G, Pál C (2017) Phenotypic heterogeneity promotes adaptive evolution. PLOS Biol 15(5):e2000644
- Boiger R, Hasenauer J, Hroß S, Kaltenbacher B (2016) Integration based profile likelihood calculation for PDE constrained parameter estimation problems. Inverse Probl 32(12):125009
- Brestoff JR, Frater JL (2022) Contemporary challenges in clinical flow cytometry: small samples, big data, little time. JALM 7(4):931–944
- Browning AP, Taşcă M, Falcó C, Baker RE (2024) Structural identifiability analysis of linear reaction-advection-diffusion processes in mathematical biology. P R Soc A 480(2286):20230911
- Browning AP, Warne DJ, Burrage K, Baker RE, Simpson MJ (2020) Identifiability analysis for stochastic differential equation models in systems biology. J R Soc Interface 17:20200652
- Burkhardt DB, San Juan BP, Lock JG, Krishnaswamy S, Chaffer CL (2022) Mapping phenotypic plasticity upon the cancer cell state landscape using manifold learning. Cancer Discov 12(8):1847–1859
- Carpenter B, Gelman A, Hoffman MD, Lee D, Goodrich B, Betancourt M, Brubaker M, Guo J, Li P, Riddell A (2017) Stan: a probabilistic programming language. J Stat Softw, 76(1)
- Cassidy T (2023) A continuation technique for maximum likelihood estimators in biological models. Bull Math Biol 85(10):90
- Cassidy T, Craig M (2019) Determinants of combination GM-CSF immunotherapy and oncolytic virotherapy success identified through in silico treatment personalization. PLOS Comput Biol 15(11):e1007495
- Cassidy T, Humphries AR (2019) A mathematical model of viral oncology as an immuno-oncology instigator. Math Med Biol A J IMA 37(1):117–151
- Cassidy T, Nichol D, Robertson-Tessi M, Craig M, Anderson ARA (2021) The role of memory in nongenetic inheritance and its impact on cancer treatment resistance. PLOS Comput Biol 17(8):e1009348
- Celora GL, Bader SB, Hammond EM, Maini PK, Pitt-Francis JM, Byrne HM (2022) A dna-structured mathematical model of cell-cycle progression in cyclic hypoxia. J Theor Biol 545:111104



- Celora GL, Byrne HM, Zois CE, Kevrekidis PG (2021) Phenotypic variation modulates the growth dynamics and response to radiotherapy of solid tumours under normoxia and hypoxia. J Theor Biol 527:110792
- Champagnat N, Ferrière R, Ben Arous G (2002) The canonical equation of adaptive dynamics: a mathematical view. Selection 2(1-2):73-83
- Champagnat N, Ferrière R, Méléard S (2006) Unifying evolutionary dynamics: from individual stochastic processes to macroscopic models. Theor Popul Biol 69(3):297-321
- Chen J-Y, Hug C, Reyes J, Tian C, Gerosa L, Fröhlich F, Ponsioen B, Snippert HJ, Spencer SL, Jambhekar A, Sorger PK, Lahav G (2023) Multi-range ERK responses shape the proliferative trajectory of single cells following oncogene induction. Cell Rep 42(3):112252
- Chisholm RH, Lorenzi T, Clairambault J (2016) Cell population heterogeneity and evolution towards drug resistance in cancer: biological and mathematical assessment, theoretical treatment optimisation. Biochim Biophys Acta 1860(11):2627-2645
- Chisholm RH, Lorenzi T, Desvillettes L, Hughes BD (2016) Evolutionary dynamics of phenotype-structured populations: from individual-level mechanisms to population-level consequences. Z Angew Math Me 67:1-34
- Chisholm RH, Lorenzi T, Lorz A (2016) Effects of an advection term in nonlocal Lotka-Volterra equations. Commun Math Sci 14(4):1181-1188
- Chisholm RH, Lorenzi T, Lorz A, Larsen AK, De Almeida LN, Escargueil A, Clairambault J (2015) Emergence of drug tolerance in cancer cell populations: an evolutionary outcome of selection, nongenetic instability, and stress-induced adaptation. Cancer Res 75(6):930-939
- Cho H, Levy D (2018) Modeling continuous levels of resistance to multidrug therapy in cancer. Appl Math Model 64:733-751
- Cho H, Levy D (2018) Modeling the chemotherapy-induced selection of drug-resistant traits during tumor growth. J Theor Biol 436:120-134
- Clairambault J, Pouchol C (2019) A survey of adaptive cell population dynamics models of emergence of drug resistance in cancer, and open questions about evolution and cancer. Biomath 8(1):23
- Coggan H, Page KM (2022) The role of evolutionary game theory in spatial and non-spatial models of the survival of cooperation in cancer: a review. J R Soc Interface, 19(193)
- Craig M, Kaveh K, Woosley A, Brown AS, Goldman D, Eton E, Mehta RM, Dhawan A, Arai K, Rahman MM, Chen S, Nowak MA, Goldman A (2019) Cooperative adaptation to therapy (CAT) confers resistance in heterogeneous non-small cell lung cancer. PLOS Comput Biol 15(8):e1007278
- Curto RE, di Dio PJ (2023) Time-dependent moments from the heat equation and a transport equation. Int Math Res Not 2023(17):14955-14990
- Dieckmann U, Law R (1996) The dynamical theory of coevolution: a derivation from stochastic ecological processes. J Math Biol 34(5-6):579-612
- Düll C, Gwiazda P, Marciniak-Czochra A, Skrzeczkowski J (2021) Spaces of measures and their applications to structured population models. Cambridge University Press, Vol. 36
- Engblom S (2006) Computing the moments of high dimensional solutions of the master equation. Appl Math Comput 180(2):498-515
- Fan S, Geissmann Q, Lakatos E, Lukauskas S, Ale A, Babtie AC, Kirk PDW, Stumpf MPH (2016) MEANS: python package for moment expansion approximation, iNference and simulation. Bioinformatics 32(18):2863-2865
- Ghusinga KR, Soltani M, Lamperski A, Dhople SV, Singh A (2017) Approximate moment dynamics for polynomial and trigonometric stochastic systems. In: 2017 IEEE 56th Annual Conference on Decision and Control (CDC), pages 1864-1869. IEEE
- Gillespie CS (2009) Moment-closure approximations for mass-action models. IET Syst Biol 3(1):52-58
- Goldman A, Majumder B, Dhawan A, Ravi S, Goldman D, Kohandel M, Majumder PK, Sengupta S (2015) Temporally sequenced anticancer drugs overcome adaptive resistance by targeting a vulnerable chemotherapy-induced phenotypic transition. Nat Commun 6(1):6139
- Greene J, Lavi O, Gottesman MM, Levy D (2014) The impact of cell density and mutations in a model of multidrug resistance in solid tumors. Bull Math Biol 76(3):627-653
- Gunnarsson EB, De S, Leder K, Foo J (2020) Understanding the role of phenotypic switching in cancer drug resistance. J Theor Biol 490:110162
- Hanahan D (2022) Hallmarks of cancer: new dimensions. Cancer Discov 12(1):31-46
- Kadanoff LP (2000) Statistical Physics: Statics. Dynamics And Renormalization, World Scientific, Singapore



Kareva I (2022) Different costs of therapeutic resistance in cancer: Short- and long-term impact of population heterogeneity. Math Biosci 352(June):108891

- Kavran AJ, Stuart SA, Hayashi KR, Basken JM, Brandhuber BJ, Ahn NG (2022) Intermittent treatment of BRAFV600E melanoma cells delays resistance by adaptive resensitization to drug rechallenge. In: Proc Natl Acad Sci USA, 119(12)
- Kaznatcheev A, Peacock J, Basanta D, Marusyk A, Scott JG (2019) Fibroblasts and alectinib switch the evolutionary games played by non-small cell lung cancer. Nat Ecol Evol 3(3):450–456
- Köhn-Luque A, Myklebust EM, Tadele DS, Giliberto M, Schmiester L, Noory J, Harivel E, Arsenteva P, Mumenthaler SM, Schjesvold F, Taskén K, Enserink JM, Leder K, Frigessi A, Foo J (2023) Phenotypic deconvolution in heterogeneous cancer cell populations using drug-screening data. Cell Rep Methods 3:100417
- Kuehn C (2016) Moment Closure—A Brief Review. In Control of Self-Organizing Nonlinear Systems, Schöll, E., Klapp, S., Hövel, P. (eds), pages 253–271. Springer
- Labrie M, Brugge JS, Mills GB, Zervantonakis IK (2022) Therapy resistance: opportunities created by adaptive responses to targeted therapies in cancer. Nat Rev Cancer 22(6):323–339
- Lavi O, Greene JM, Levy D, Gottesman MM (2013) The role of cell density and intratumoral heterogeneity in multidrug resistance. Cancer Res 73(24):7168–7175
- Lee CH, Kim K-H, Kim P (2009) A moment closure method for stochastic reaction networks. J Chem Phys. 130(13)
- Lorenzi T, Chisholm RH, Desvillettes L, Hughes BD (2015) Dissecting the dynamics of epigenetic changes in phenotype-structured populations exposed to fluctuating environments. J Theor Biol 386:166–176
- Lorenzi T, Macfarlane FR, Villa C (2020) Discrete and continuum models for the evolutionary and spatial dynamics of cancer: a very short introduction through two case studies. In Trends in Biomathematics: Modeling Cells, Flows, Epidemics, and the Environment, pages 359–380. Springer
- Marine J-C, Dawson S-J, Dawson MA (2020) Non-genetic mechanisms of therapeutic resistance in cancer. Nat Rev Cancer 20(12):743–756
- Martinez VA, Laleh NG, Salvioli M, Thuijsman F, Brown JS, Cavill R, Kather JN, Staňková K (2021) Improving mathematical models of cancer by including resistance to therapy: a study in non-small cell lung cancer. bioRxiv, pages 1–27
- Marusyk A, Janiszewska M, Polyak K (2020) Intratumor heterogeneity: the rosetta stone of therapy resistance. Cancer cell 37(4):471–484
- McGranahan N, Swanton C (2017) Clonal heterogeneity and tumor evolution: past, present, and the future. Cell 168(4):613–628
- Mosier JA, Schwager SC, Boyajian DA, Reinhart-King CA (2021) Cancer cell metabolic plasticity in migration and metastasis. Clin Exp Metastasis 38(4):343–359
- Nichol D, Robertson-Tessi M, Jeavons P, Anderson AR (2016) Stochasticity in the genotype-phenotype map: implications for the robustness and persistence of bet-hedging. Genetics 204(4):1523–1539
- Oshternian SR, Loipfinger S, Bhattacharya A, Fehrmann RSN (2024) Exploring combinations of dimensionality reduction, transfer learning, and regularization methods for predicting binary phenotypes with transcriptomic data. BMC Bioinform 25(1):167
- Perthame B (2006) Transport equations in biology. Springer Science & Business Media, Birkhäuser Verlag, Basel, Boston, Berlin
- Perthame B, Barles G (2008) Dirac concentrations in Lotka-Volterra parabolic PDEs. Indiana U Math J 57(7):3275–3301
- Pigliucci M (2010) Genotype-phenotype mapping and the end of the 'genes as blueprint' metaphor. Philos Trans R Soc B 365(1540):557–566
- Pressley M, Salvioli M, Lewis DB, Richards CL, Brown JS, Staňková K (2021) Evolutionary dynamics of treatment-induced resistance in cancer informs understanding of rapid evolution in natural systems. Front Ecol Evol 9(August):1–22
- Raue A, Kreutz C, Maiwald T, Bachmann J, Schilling M, Klingmüller U, Timmer J (2009) Structural and practical identifiability analysis of partially observed dynamical models by exploiting the profile likelihood. Bioinformatics 25(15):1923–1929
- Schnoerr D, Sanguinetti G, Grima R (2017) Approximation and inference methods for stochastic biochemical kinetics—a tutorial review. J Phys A 50(9):093001
- Shaffer SM, Dunagin MC, Torborg SR, Torre EA, Emert B, Krepler C, Beqiri M, Sproesser K, Brafford PA, Xiao M, Eggan E, Anastopoulos IN, Vargas-Garcia CA, Singh A, Nathanson KL, Herlyn M, Raj A (2017) Rare cell variability and drug-induced reprogramming as a mode of cancer drug resistance. Nature 546(7658):431–435



- Sharma SV, Lee DY, Li B, Quinlan MP, Takahashi F, Maheswaran S, McDermott U, Azizian N, Zou L, Fischbach MA, Wong KK, Brandstetter K, Wittner B, Ramaswamy S, Classon M, Settleman J (2010) A chromatin-mediated reversible drug-tolerant state in cancer cell subpopulations. Cell 141(1):69–80
- Shen S, Clairambault J (2020) Cell plasticity in cancer cell populations. F1000Research, 9:F1000 Faculty Rev-635
- Shi Z-D, Pang K, Wu Z-X, Dong Y, Hao L, Qin J-X, Wang W, Chen Z-S, Han C-H (2023) Tumor cell plasticity in targeted therapy-induced resistance: mechanisms and new strategies. Signal Transduct Target Ther 8(1):113
- Smalley I, Kim E, Li J, Spence P, Wyatt CJ, Eroglu Z, Sondak VK, Messina JL, Babacan NA, Maria-Engler SS et al (2019) Leveraging transcriptional dynamics to improve braf inhibitor responses in melanoma. EBioMedicine 48:178-190
- Smith S, Fox R, Raman V (2007) A quadrature closure for the reaction-source term in conditional-moment closure. Proc Combust Inst 31(1):1675-1682
- Sottoriva A, Spiteri I, Piccirillo SGM, Touloumis A, Collins VP, Marioni JC, Curtis C, Watts C, Tavaré S (2013) Intratumor heterogeneity in human glioblastoma reflects cancer evolutionary dynamics. Proc Natl Acad Sci USA 110(10):4009-4014
- Stace RE, Stiehl T, Chaplain MA, Marciniak-Czochra A, Lorenzi T (2020) Discrete and continuum phenotype-structured models for the evolution of cancer cell populations under chemotherapy. Math Model Nat Phenom 15:14
- Stapor P, Weindl D, Ballnus B, Hug S, Loos C, Fiedler A, Krause S, Hroß S, Fröhlich F, Hasenauer J (2018) PESTO: Parameter Estimation Toolbox. Bioinformatics 34(4):705–707
- Tang KL, Li TH, Xiong WW, Chen K (2010) Ovarian cancer classification based on dimensionality reduction for SELDI-TOF data. BMC Bioinformatics 11:109
- Tasdogan A, Faubert B, Ramesh V, Ubellacker JM, Shen B, Solmonson A, Murphy MM, Gu Z, Gu W, Martin M et al (2020) Metabolic heterogeneity confers differences in melanoma metastatic potential. Nature 577(7788):115-120
- Tirosh I, Izar B, Prakadan SM, Wadsworth MH, Treacy D, Trombetta JJ, Rotem A, Rodman C, Lian C, Murphy G, Fallahi-Sichani M, Dutton-Regester K, Lin J-R, Cohen O, Shah P, Lu D, Genshaft AS, Hughes TK, Ziegler CGK, Kazer SW, Gaillard A, Kolb KE, Villani A-C, Johannessen CM, Andreev AY, Van Allen EM, Bertagnolli M, Sorger PK, Sullivan RJ, Flaherty KT, Frederick DT, Jané-Valbuena J, Yoon CH, Rozenblatt-Rosen O, Shalek AK, Regev A, Garraway LA (2016) Dissecting the multicellular ecosystem of metastatic melanoma by single-cell RNA-seq. Science 352(6282):189-196
- Villa C, Chaplain MA, Lorenzi T (2021) Evolutionary dynamics in vascularised tumours under chemotherapy: mathematical modelling, asymptotic analysis and numerical simulations. Vietnam J Math 49:143-167
- Vincent TL, Brown JS (2005) Evolutionary game theory, natural selection, and darwinian dynamics. Cambridge University Press, Cambridge
- Vincent TL, Gatenby RA (2008) An evolutionary model for initiation, promotion, and progression in carcinogenesis. Int J Oncol 32(4):729-37
- Vogelstein JT, Bridgeford EW, Tang M, Zheng D, Douville C, Burns R, Maggioni M (2021) Supervised dimensionality reduction for big data. Nat Commun 12(1):2872
- Wagner V, Castellaz B, Oesting M, Radde N (2022) Quasi-entropy closure: a fast and reliable approach to close the moment equations of the chemical master equation. Bioinformatics 38(18):4352-4359
- West J, Ma Y, Newton PK (2018) Capitalizing on competition: an evolutionary model of competitive release in metastatic castration resistant prostate cancer treatment. J Theor Biol 455:249-260
- Xue Y, Martelotto L, Baslan T, Vides A, Solomon M, Mai TT, Chaudhary N, Riely GJ, Li BT, Scott K, Cechhi F, Stierner U, Chadalavada K, de Stanchina E, Schwartz S, Hembrough T, Nanjangud G, Berger MF, Nilsson J, Lowe SW, Reis-Filho JS, Rosen N, Lito P (2017) An approach to suppress the evolution of resistance in BRAF[CDATA[$^{\rm N}$ V600E }]]V600E-mutant cancer. Nat Med 23(8):929-937

Publisher's Note Springer Nature remains neutral with regard to jurisdictional claims in published maps and institutional affiliations.



22 Page 32 of 32 C. Villa et al.

Authors and Affiliations

Chiara Villa^{1,2} · Philip K. Maini³ · Alexander P. Browning³ · Adrianne L. Jenner⁴ · Sara Hamis^{5,6} · Tyler Cassidy⁷

- ☐ Chiara Villa chiara.villa@inria.fr
- ☐ Tyler Cassidy t.cassidy1@leeds.ac.uk
- Université Paris-Saclay, Inria, Centre Inria de Saclay, Palaiseau 91120, France
- Sorbonne Université, CNRS, Université de Paris, Laboratoire Jacques-Louis Lions, UMR 7598, 75005 Paris, France, Paris, France
- Mathematical Institute, University of Oxford, Oxford, UK
- School of Mathematical Sciences, Queensland University of Technology, Brisbane, Australia
- ⁵ Department of Information Technology, Uppsala University, Uppsala, Sweden
- Faculty of Medicine and Health Technology, Tampere University, Tampere, Finland
- School of Mathematics, University of Leeds, Leeds, UK

